



# The effect of graphene on the activation energy of grain growth for the nanocrystalline thermoelectric n-type $\text{Bi}_2\text{Te}_{2.7}\text{Se}_{0.3}$

Farah M. El-Makaty<sup>1</sup> · Nandagopal S. Pothuvattil<sup>2</sup> · Abdelmagid Hamouda<sup>1</sup> · Khaled M. Youssef<sup>3</sup>

Received: 27 May 2022 / Accepted: 20 September 2022  
© The Author(s) 2022

## Abstract

Even though bismuth telluride is frequently produced by mechanical alloying for thermoelectric materials, no data has been published addressing the thermal behavior and activation energy of the milled n-type  $\text{Bi}_2\text{Te}_{2.7}\text{Se}_{0.3}$  powders. This paper studies the activation energy of grain growth for the nanocrystalline n-type  $\text{Bi}_2\text{Te}_{2.7}\text{Se}_{0.3}$  and two graphene- $\text{Bi}_2\text{Te}_{2.7}\text{Se}_{0.3}$  composites with different graphene concentrations (0.05 and 0.5 wt.%). Grain size and structural analyses of these samples have been carried out using X-ray diffraction (XRD) and transmission electron microscopy (TEM). The thermal stability of the three samples is investigated by incorporating differential scanning calorimetry data with the Kissinger model. The activation energy of the pristine  $\text{Bi}_2\text{Te}_{2.7}\text{Se}_{0.3}$  alloy is found to be 268 kJ/mol. For the composite samples, a lower graphene weight percentage (0.05 wt.%) increased the activation energy to 270 kJ/mol. In contrast, higher amounts of graphene (0.5 wt.%) reduced the activation energy significantly to 254 kJ/mol. The observed effect is found to be directly related to graphene's exfoliation in the bismuth telluride matrix. These results offer a better understanding of the thermal behavior of the nanocrystalline pristine n-type  $\text{Bi}_2\text{Te}_{2.7}\text{Se}_{0.3}$  and the influence of graphene nanofiller on the thermal stability of the bismuth telluride nanocomposites.

**Keywords** Activation energy · Grain growth · Mechanical milling · Bismuth telluride · Graphene

## 1 Introduction

The solid solutions of the inorganic n-type bismuth telluride ( $\text{Bi}_2(\text{Te}_{1-\delta}\text{Se}_\delta)_3$ ) are widely applied in thermoelectric devices due to their unrivaled thermoelectric properties at low temperatures [1]. Enhancements in the thermoelectric properties through nanostructuring have been reported to further boost the efficiency by increasing phonon scattering at the newly introduced grain boundaries [1]. Moreover, it is reported that reducing the grain size to the nanoscale regime improves the physical and mechanical properties of the material considerably [2, 3]. However, these nanostructures are inherently

unstable at elevated temperatures because the nanograins provide a very large driving force for grain growth [4].

Ball milling is a quick, economical, and widely used method for preparing nanomaterials, including bismuth telluride [5, 6]. However, the ball-milled powders must be consolidated for thermoelectric properties measurement and to be employed in devices. The most common consolidation techniques use high temperatures to allow for the diffusion of particles to take place. Such methods include spark plasma sintering, plasma-activated sintering, microwave sintering, hot pressing, and hot isostatic pressing [7, 8]. For bismuth telluride, the compaction of milled powders is usually done in temperatures ranging from 300 to 450 °C [9–15]. Since the temperature and heating rate can vary substantially, developing an understanding of the behavior of grain growth is one of the critical aspects of designing nanomaterials.

Nanocrystalline materials are inherently unstable at elevated temperature because the nano-scale grain size provides a very large driving force for grain growth. It is well accepted that the most dominant characteristic of ball-milled nanomaterials is their high specific boundary area, which increases the driving force for grain growth. In spite

✉ Khaled M. Youssef  
kyoussef@qu.edu.qa

<sup>1</sup> Mechanical and Industrial Engineering Department, Qatar University, 2713 Doha, Qatar

<sup>2</sup> Central Laboratory Unit, Qatar University, 2713 Doha, Qatar

<sup>3</sup> Materials Science and Technology Graduate Program, Department of Mathematics, Statistics, and Physics, College of Arts and Sciences, Qatar University, 2713 Doha, Qatar

of the greater vulnerability to coarsening in nanomaterials, recrystallization is usually repressed by the high amount of accumulated enthalpy within the grain boundaries [16]. Mechanical milling also creates high amount of defects, leading to excess free volume and non-equilibrium grain boundaries [17]. The mentioned phenomena speak the need for a detailed investigation of grain growth kinetics in ball-milled  $\text{Bi}_2\text{Te}_3$  nanomaterials. However, the activation energy of grain growth for bismuth telluride has been seldomly reported. Humphry-Baker et al. [16] studied the grain growth of ball-milled  $\text{Bi}_2\text{Te}_3$  and reported activation energy of 242 kJ/mol that is controlled by diffusional grain boundary migration above a homologous temperature of 230 °C. The authors constructed a thermal budget map to offer suggestions for enhancing the thermoelectric properties of nanomaterials prepared through powder routes. Such knowledge offers a guideline for designing consolidation approaches that lessen grain growth and produce more stable materials. It would also be critical in practical applications, as thermoelectric generators based on ball-milled  $\text{Bi}_2\text{Te}_3$  will be exposed to severe, long-lasting thermal excursions.

Even though the preparation of various bismuth telluride compositions using ball milling followed by consolidation has been successfully applied, and the thermoelectric properties have been investigated [5, 6], the kinetics of the ball-milled powders for the doped n-type bismuth telluride has not been reported yet. Herein, the effect of heat and heating rate on the grain growth of the most synthesized n-type bismuth telluride composition,  $\text{Bi}_2\text{Te}_{2.7}\text{Se}_{0.3}$ , is explored. The effect of the addition of two different graphene concentrations on the activation energy of grain growth is also investigated. The activation energy of all the samples is calculated using the Kissinger model.

## 2 Methodology

### 2.1 Materials and synthesis of $\text{Bi}_2\text{Te}_{2.7}\text{Se}_{0.3}$ and GNS- $\text{Bi}_2\text{Te}_{2.7}\text{Se}_{0.3}$ composites

Elemental powders of bismuth (99.99%, Sigma-Aldrich, Germany), tellurium (99.997%, Sigma-Aldrich, Germany), and selenium (99.5%, Alfa Aesar, Germany) were used to prepare a pristine n-type sample according to the formula  $\text{Bi}_2\text{Te}_{2.7}\text{Se}_{0.3}$ . The powders were milled in a stainless steel vial under an ultra-high-purity argon atmosphere ( $\text{O}_2 < 0.5$  ppm) via a SPEX milling device (SamplePrep, 8000 M, New Jersey) for 20 h with a ball to powder ratio of 7:1. Graphene nanosheets (GNS) (Sigma-Aldrich, Germany) were utilized, following the same conditions of the pristine sample, to prepare two GNS- $\text{Bi}_2\text{Te}_{2.7}\text{Se}_{0.3}$  composites. The amounts of GNS used in the composites are 0.5 and 0.05 wt.%. In the GNS- $\text{Bi}_2\text{Te}_{2.7}\text{Se}_{0.3}$  composite samples,

GNS was added at the last 10 min of mechanical milling. In order to study the grain growth, the milled powders were annealed from RT until 380 °C using a tube furnace (GSL-1500X-RTP50, California) at 10 °C/min under mixed gas (2% hydrogen, 98% argon) with an absolute pressure of 0.04 MPa. As demonstrated later, 380 °C is the peak temperature for grain growth, making this annealing temperature convenient for the present study. The samples were immediately removed from the furnace once the desired temperature (380 °C) was reached and cooled under mixed gas flow.

### 2.2 Characterization

Phase identification and grain size determination of the as-milled and annealed samples were conducted by X-ray diffraction (XRD: PANalytical, EMPYREAN, UK) using a radiation source of  $\text{Cu}/\text{K}\alpha$  ( $\lambda = 1.54$  Å). The morphology of the as-milled samples was analyzed via scanning electron microscopy (SEM) (Nano-SEM Nova 450, FEI-USA). Vickers microhardness (HV) (Future-Tech, FM-ARS900, Japan) was carried out for as-milled and annealed powders using 25gf and a dwelling time of 10 s, performing at least eight indentations for each sample. By measuring the HV, the effect of annealing on the stored energy as well as stresses (e.g., milling-induced stresses) is revealed. The structural features of the powder samples were further investigated, and the grain size was confirmed using a transmission electron microscope (TEM) (Tecnai G2 FEG 200 kV, FEI, Spain). The TEM samples were prepared by sonicating in isopropyl alcohol using an ultra-sonicator bath for 20 min. The sonicated material was then drop-casted onto a 300-mesh carbon film-covered copper grid. The thermal behavior of as-milled powder samples was studied by differential scanning calorimetry (DSC) (PerkinElmer, DSC 4000, UK) at different heating rates of 5, 10, 20, 30 and 40 °C/min from room temperature up to 430 °C under an ultra-high-purity argon atmosphere. The thermal scans were repeated two times, and the error in  $\Delta H$  was less than 11%.

## 3 Results and discussion

In order to study the morphology of the as-milled sample, SEM was performed, and the images are shown in Fig. 1. As-received GNS shown in Fig. 1a reveals the typical graphene nanosheets in agglomerated form. Pristine  $\text{Bi}_2\text{Te}_{2.7}\text{Se}_{0.3}$ , shown in Fig. 1b, illustrates refined and irregular particles of the as-milled powders. Figure 1c and 1d is the SEM images for GNS- $\text{Bi}_2\text{Te}_{2.7}\text{Se}_{0.3}$  composites with 0.05 and 0.5 wt.% GNS, respectively. GNS are present and marked with red arrows. Mainly, both composites display matching particle-like morphology of the n-type  $\text{Bi}_2\text{Te}_{2.7}\text{Se}_{0.3}$  matrix entwined with graphene. By comparison, the former composite (0.05

wt.%) has a small amount of GNS layers in-between the particles, while the latter one (0.5 wt.%) clearly shows high concentrations of agglomerated GNS.

Figure 2 presents the thermal behavior of the as-milled samples studied via DSC using a heating rate of 10 °C/min. The patterns of all samples show two main peaks. The first peak is an exothermic reaction starting at 373 °C and ending at 394 °C, whereas the second peak is an endothermic reaction representing a melting process around 415 °C. This

endothermic reaction could be attributed to the melting of the eutectic composition between bismuth and tellurium, as reported in the literature [18]. In order to investigate the exothermic reaction, the as-milled samples were annealed until the exothermic peak temperature ( $T = 380$  °C), then examined using X-ray diffraction and Vickers microhardness.

The XRD patterns before and after annealing the as-milled samples are illustrated in Fig. 3a and 3b, respectively. It is clearly seen that only characteristic peaks from

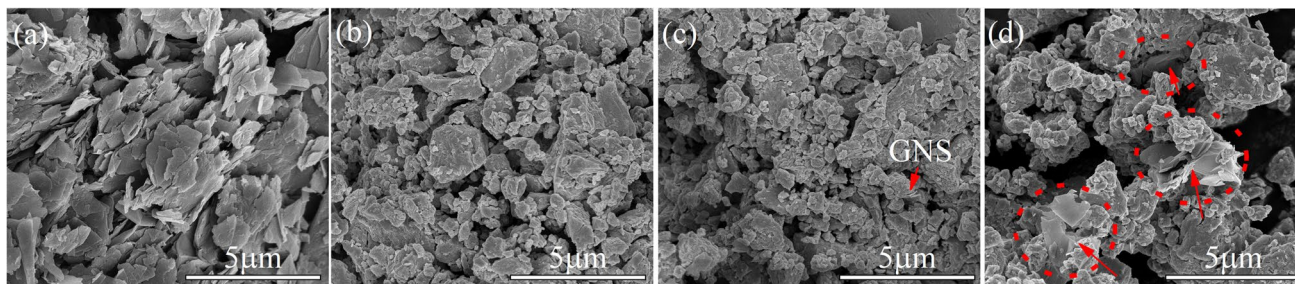


Fig. 1 SEM images for (a) as-received GNS and as-milled (b)  $\text{Bi}_2\text{Te}_{2.7}\text{Se}_{0.3}$ , (c) 0.05wt.%GNS- $\text{Bi}_2\text{Te}_{2.7}\text{Se}_{0.3}$ , and (d) 0.5wt.%GNS- $\text{Bi}_2\text{Te}_{2.7}\text{Se}_{0.3}$  samples

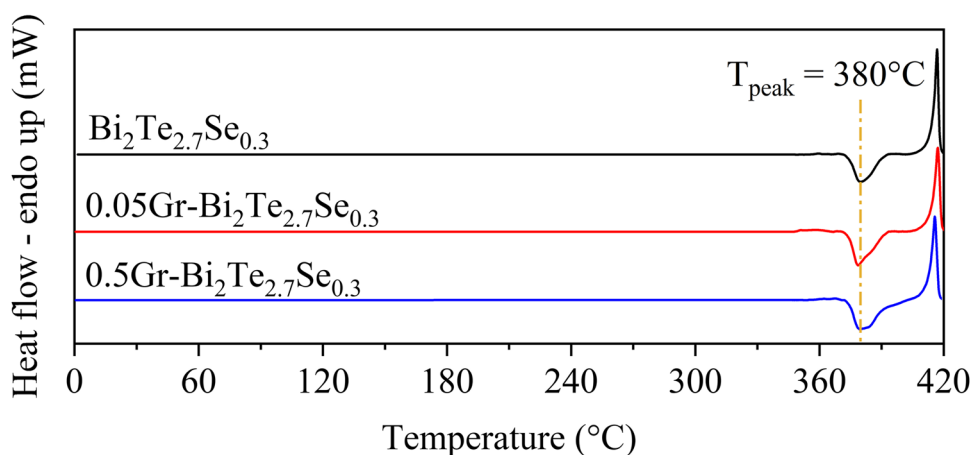


Fig. 2 Thermal analysis of the as milled samples at 10 °C/min

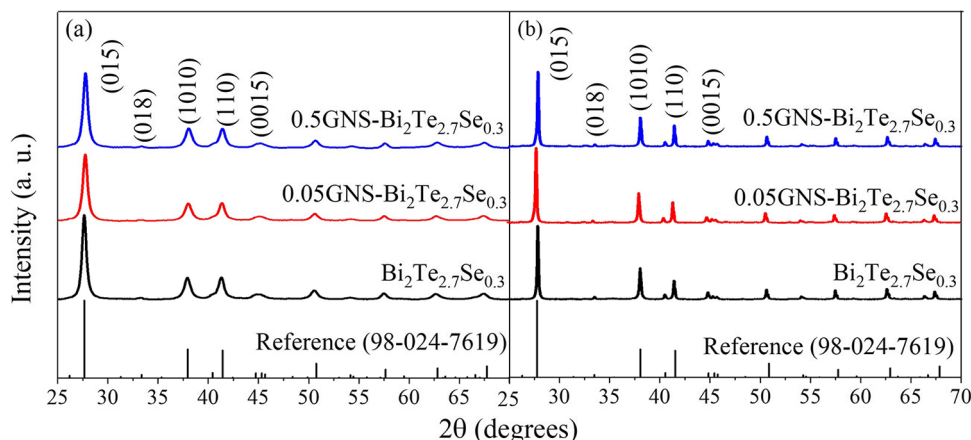


Fig. 3 XRD diagram for (a) as-milled powders, (b) annealed samples at 10 °C/min to 380 °C and the reference card number 98-024-7619 presented for doped n-type  $\text{Bi}_2\text{Te}_{2.7}\text{Se}_1$  [19]

$\text{Bi}_2\text{Te}_{2.7}\text{Se}_{0.3}$  are present (card no. 98–024–7619 [19]), and no peaks for graphene are observed in the samples. Wang et al. [20] has observed similar phenomenon with  $\text{Al}_2\text{O}_3/\text{WC}/\text{TiC}/\text{graphene}$  composite and explained that such low volume fraction of graphene was beyond the detection limit of XRD. It is also noticed that the peaks became sharper after the annealing, indicating an increase in the grain size and strain release [16]. The integral breadth analysis was used to calculate the grain size and lattice micro-strain from the XRD line broadening [21]. This analysis presumes that grain size and lattice strain broadening profiles can be approximated by Cauchy and Gaussian functions, respectively, leading to the following equation [21]:

$$\frac{\beta_{hkl}^2}{\tan^2 \theta} = \frac{\lambda}{D} \left( \frac{\beta_{hkl}}{\tan \theta \sin \theta} \right) + 25 \langle \epsilon^2 \rangle \quad (1)$$

where  $\beta_{hkl}$  is the width of the peak at half-maximum intensity,  $\lambda$  is the wavelength of the x-ray beam,  $\theta$  is the peak position,  $D$  is the average grain size, and  $\epsilon$  is the lattice strain. Fitting  $\beta_{hkl}^2/\tan^2\theta$  against  $\beta_{hkl}/(\tan\theta \sin\theta)$  gave a linear regression fit  $R > 0.91$  for all measurements. The data of the calculated  $D$  and  $\epsilon$  are shown in Table 1. As-milled powders had similar grain size value of about 12 nm. After annealing, the grain size increased to about 62 nm. The noticed increase (~50 nm) defines the exothermic peak at 380 °C as grain growth. Grain growth due to the heat treatment of milled powder agrees with previous results. Zhang et al. [21] reported a grain size of 10 nm for ball-milled p-type  $\text{Bi}_{0.4}\text{Sb}_{1.6}\text{Te}_3$ . After heat treating the sample at 450 °C for 2 min, the authors noticed an increase in grain size to 200 nm. Besides, the lattice strain (in Table 1) has noticeably decreased after annealing the milled samples. The released strain can be explained by the excess energy resulting from the non-equilibrium ball milling technique [22]. Hence, the exothermic reaction also contributed to stabilizing the lattice structure of the milled phase.

To further understand the effect of annealing on the prepared samples, microhardness tests were performed, and the results are shown in Fig. 4. A clear drop in the microhardness of the annealed samples (compared to as-milled

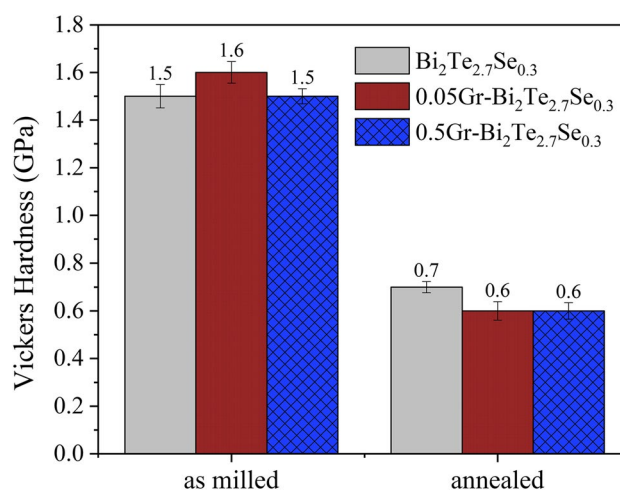


**Fig. 4** Vickers microhardness values for as-milled powders and annealed samples at 10 °C/min to 380 °C

powders) is present. This trend has also been found in literature where Ahmed et al. [23] investigated the thermal stability of nanocrystalline Al-Li-Sr graphene alloys prepared by mechanical milling then annealing isothermally at different temperatures. The reported microhardness data before and after annealing revealed a clear reduction from 2.1 GPa for as-milled powder to 1.1 GPa after annealing at 500 °C for 1 h. This drop in microhardness was explained by the reduction of total area of grain boundary due to grain growth and recovery. Hence, this may suggest that the microhardness drop observed in our study indicates a lower amount of defects (mostly milling-induced defects) and/or less volume fraction of grain boundaries [24]. Defects and grain boundaries act as a restriction for dislocation motion, stimulating stress build-up within the material. Therefore, when the nanocrystalline  $\text{Bi}_2\text{Te}_{2.7}\text{Se}_{0.3}$  alloy is heated to 380 °C (grain growth peak), the grain size increases through the diffusion of grain boundaries and stresses due to milling-induced defects are released. This leads to lower hardness, an increase in the grain size, and reduced lattice strain of the nanopowders.

To confirm the grain size evaluated using the integral breadth analysis and further explore the structure, as-milled 0.5wt.%GNS- $\text{Bi}_2\text{Te}_{2.7}\text{Se}_{0.3}$  sample was investigated via TEM, and the results are shown in Fig. 5. Figure 5a presents the bright-field (BF) TEM image of the composite showing GNS attached to the n-type  $\text{Bi}_2\text{Te}_{2.7}\text{Se}_{0.3}$  matrix. The nanostructure of this composite particle is investigated using bright-field, dark-field (DF) TEM images and the electron diffraction pattern (Figs. 5b-d). While the dark field TEM image shows homogeneous equiaxed nanograins, the diffraction pattern reveals random orientations of the pseudohexagonal  $\text{Bi}_2\text{Te}_{2.7}\text{Se}_{0.3}$  grains and atomic planes. These indexed atomic planes in Fig. 5d match well with the XRD results (Fig. 3a). Figure 5e shows a monotonic grain size

**Table 1** Integral breadth analysis for grain size calculations of pristine and GNS/ $\text{Bi}_2\text{Te}_{2.7}\text{Se}_{0.3}$

Sample	Grain Size (nm)	Strain (%)
Milled $\text{Bi}_2\text{Te}_{2.7}\text{Se}_{0.3}$	13	0.383
Milled 0.05wt.%GNS- $\text{Bi}_2\text{Te}_{2.7}\text{Se}_{0.3}$	12	0.284
Milled 0.5wt.%GNS- $\text{Bi}_2\text{Te}_{2.7}\text{Se}_{0.3}$	12	0.348
Annealed $\text{Bi}_2\text{Te}_{2.7}\text{Se}_{0.3}$	62	0.103
Annealed 0.05wt.%GNS- $\text{Bi}_2\text{Te}_{2.7}\text{Se}_{0.3}$	60	0.099
Annealed 0.5wt.%GNS- $\text{Bi}_2\text{Te}_{2.7}\text{Se}_{0.3}$	65	0.104

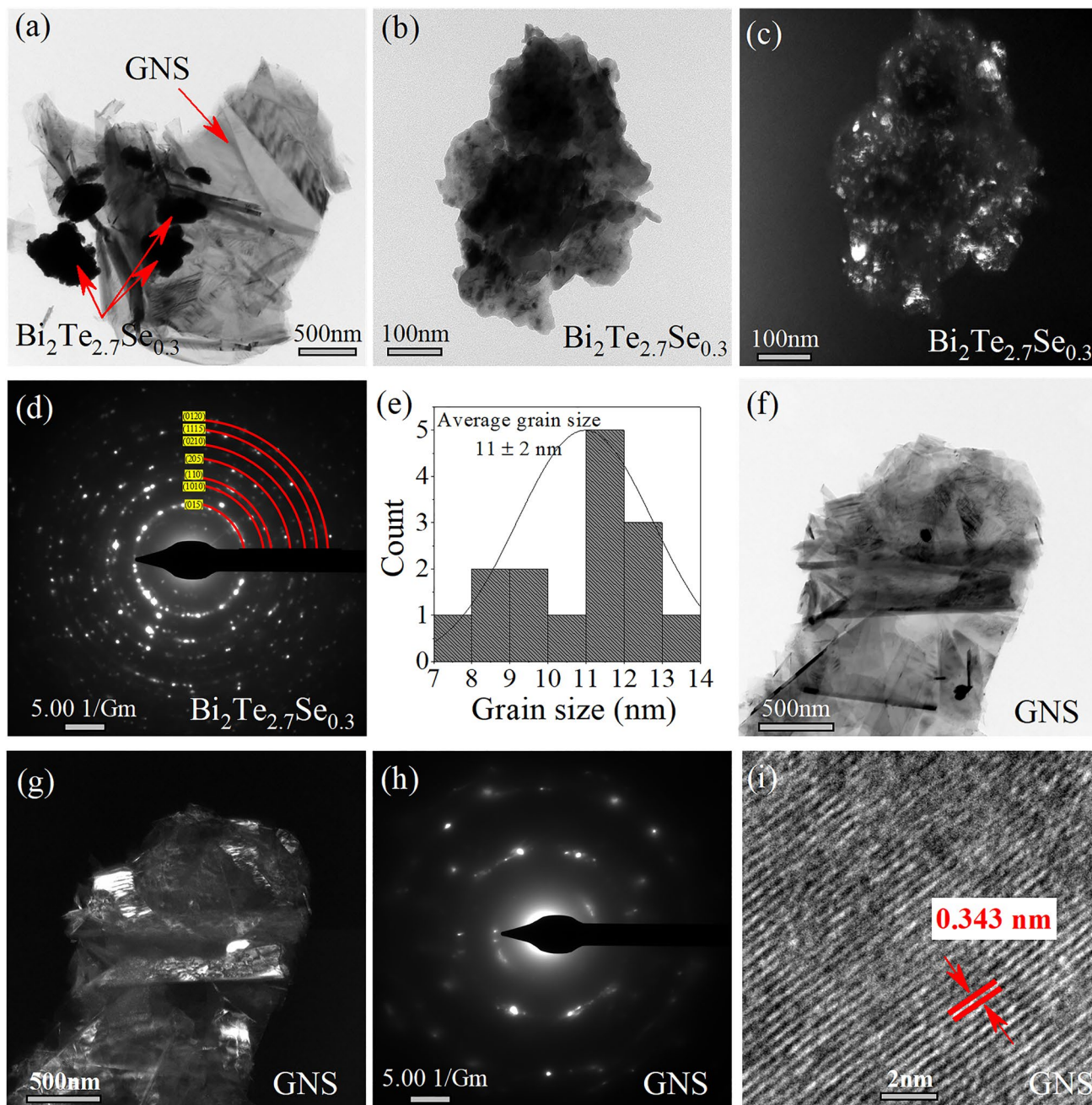


**Fig. 5** TEM analysis for as milled 0.5wt.%GNS- $\text{Bi}_2\text{Te}_{2.7}\text{Se}_{0.3}$  sample showing (a) a representative BF-TEM image for the composite, (b) BF, (c) DF, (d) diffraction pattern, and (e) grain size distribution for

an n-type bismuth telluride particle, and (f) BF, (g) DF, (h) diffraction pattern, and (i) HRTEM image for a GNS

distribution obtained from several dark-field TEM images with an average grain size of  $11 \pm 2$  nm. That grain size value matches the grain size for the as milled 0.5wt.% GNS- $\text{Bi}_2\text{Te}_{2.7}\text{Se}_{0.3}$  obtained from XRD data.

A set of BF-TEM, DF-TEM images, and diffraction patterns from a single GNS along with a high-resolution TEM (HRTEM) is shown in Fig. 5f-i. The BF-TEM image shows overlapped and folded GNS that has been reported to form as

a result of the impact forces during mechanical milling [25]. The diffraction pattern reveals polycrystalline structure, suggesting multilayered graphene, hence confirming the prior SEM observation of agglomerated and overlapped GNS in the sample. The multilayered diffraction pattern of GNS is in agreement with the results obtained by Lin et al. [25]. The authors studied solvent-assisted liquid-phase exfoliation and electrochemical exfoliation of graphite. Low exfoliation in

the liquid-phase route resulted in a polycrystalline diffraction pattern of multilayered graphene, while enhanced exfoliation by the electrochemical process exhibited the typical sixfold symmetric diffraction pattern of single-layered graphene. The HR-TEM image in Fig. 5i verifies the interplanar spacing of graphene, which is well reported to be 0.343 [26].

In order to examine the structure of the GNS in the other as-milled composite, a BF-TEM image, a DF-TEM image, and diffraction pattern for the GNS from 0.05wt.%GNS-Bi<sub>2</sub>Te<sub>2.7</sub>Se<sub>0.3</sub> sample were obtained (Fig. 6). Compared to the previous sample (0.5wt.%GNS-Bi<sub>2</sub>Te<sub>2.7</sub>Se<sub>0.3</sub>), less folding is observed in this GNS, indicating fewer milling induced defects [25]. The diffraction pattern in Fig. 6c matches with few-layered graphene, supporting the discussed observations. Hence, compositing Bi<sub>2</sub>Te<sub>2.7</sub>Se<sub>0.3</sub> with low amounts of GNS (0.05 wt.%) lowers the concentration of defects and folding, while high weight percentages (0.5 wt.%) leads to overlapping and agglomeration of GNS.

Even though integral breadth analysis is useful for calculating grain size at low nanoscale range (< 30 nm), this method becomes inaccurate for larger grain size [27]. Thus, TEM imaging was done for the samples after annealing to obtain precise grain size analysis (Fig. 7). Grain size taken by tracing grains from several dark-field images revealed that 0.05wt.%GNS-Bi<sub>2</sub>Te<sub>2.7</sub>Se<sub>0.3</sub> sample encountered lower grain growth (~29 nm) compared to pristine Bi<sub>2</sub>Te<sub>2.7</sub>Se<sub>0.3</sub> sample (~36 nm). On the other hand, severe grain growth (~130 nm) occurred in 0.5wt.% GNS-Bi<sub>2</sub>Te<sub>2.7</sub>Se<sub>0.3</sub> sample. It is noteworthy that a good agreement in the trend exists between XRD and TEM grain size measurements, even though the error in grain size is high and varies with the samples.

The value of activation energy is important as it can bring insight into the mechanism and resistance to grain growth. Grain growth kinetics were investigated through DSC using different heating rates of 5, 10, 20, 30, and 40 °C/min. The results for the samples Bi<sub>2</sub>Te<sub>2.7</sub>Se<sub>0.3</sub>, 0.05wt.% Gr-Bi<sub>2</sub>Te<sub>2.7</sub>Se<sub>0.3</sub>, and 0.5wt.% Gr-Bi<sub>2</sub>Te<sub>2.7</sub>Se<sub>0.3</sub>, are illustrated in Fig. 8a, b, and c, respectively. It is observed that as the heating rate increases, the grain growth peak shifts to a higher

temperature. This observation is consistent with the reported data by Han et al. [7] for sintered p-type Bi<sub>2</sub>Te<sub>3</sub> prepared by ball milling and melt spinning. The shift was explained as lower heating rates take longer exposure time leading to prior grain growth peaks. The activation energy of the grain growth,  $E_a$ , was calculated using the Kissinger model [24] shown in Eq. (2):

$$\ln\left(\frac{\beta}{T^2}\right) = \ln\left(\frac{AR}{E_a}\right) - \frac{E_a}{RT} \quad (2)$$

Where  $\beta$  is the heating rate,  $T$  is the onset temperature in K,  $A$  is the preexponential factor, and  $R$  is the universal gas constant [28]. The activation energies of the samples were then calculated from the slope of  $\ln(\beta/T^2)$  versus  $1/T$  plot, shown in the inset of Fig. 5a–c.

For the pristine Bi<sub>2</sub>Te<sub>2.7</sub>Se<sub>0.3</sub>, the activation energy was found to be 268 kJ/mol. In comparison with other nanostructuring techniques, non-equilibrium ball-milled powders have a high amount of energy accommodated as defects and dislocations, allowing for greater storage of enthalpy. Thus, the total activation energy accounts for reordering of the grain interior as well as relaxation of grain boundary [16]. Compared to the activation energy of grain growth for ball-milled Bi<sub>2</sub>Te<sub>3</sub> reported by Humphry-Baker et al. [16] of 242 kJ/mol, the obtained value is higher. This can be attributed to the effect of the n-type Se doping, which increases the density of antisite defects within the material [29]. Moreover, the parameters used during the milling process significantly affect the microstructure of the prepared material and the number of defects introduced [30]. The undoped milled Bi<sub>2</sub>Te<sub>3</sub> powders reported by Humphry-Baker et al. were milled using milling balls of 1.5 g, whereas, in this study, 49 g were used. This might be another reason for increasing the defects in our case, leading to higher stored energy.

The effect of graphene on the activation energy of grain growth for the pristine Bi<sub>2</sub>Te<sub>2.7</sub>Se<sub>0.3</sub> is investigated using two different weight percentages of 0.05 and 0.5. As the insets in Fig. 8 show, adding a small amount of graphene

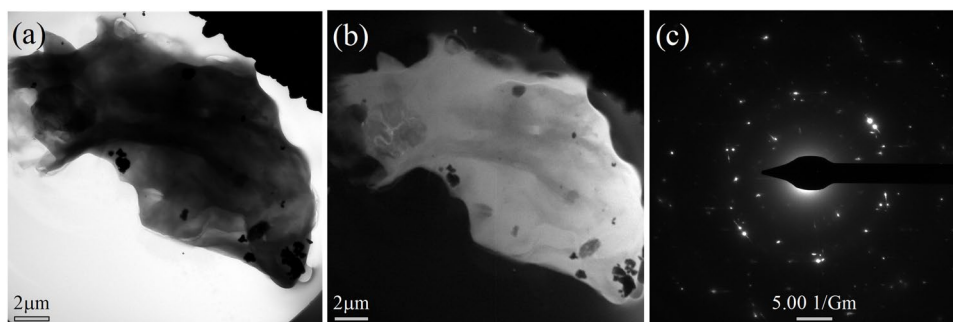


**Fig. 6** TEM analysis for as milled 0.05wt.%GNS-Bi<sub>2</sub>Te<sub>2.7</sub>Se<sub>0.3</sub>, showing (a) a BF-TEM image, (b) a DF-TEM image, and (c) diffraction pattern for the GNS

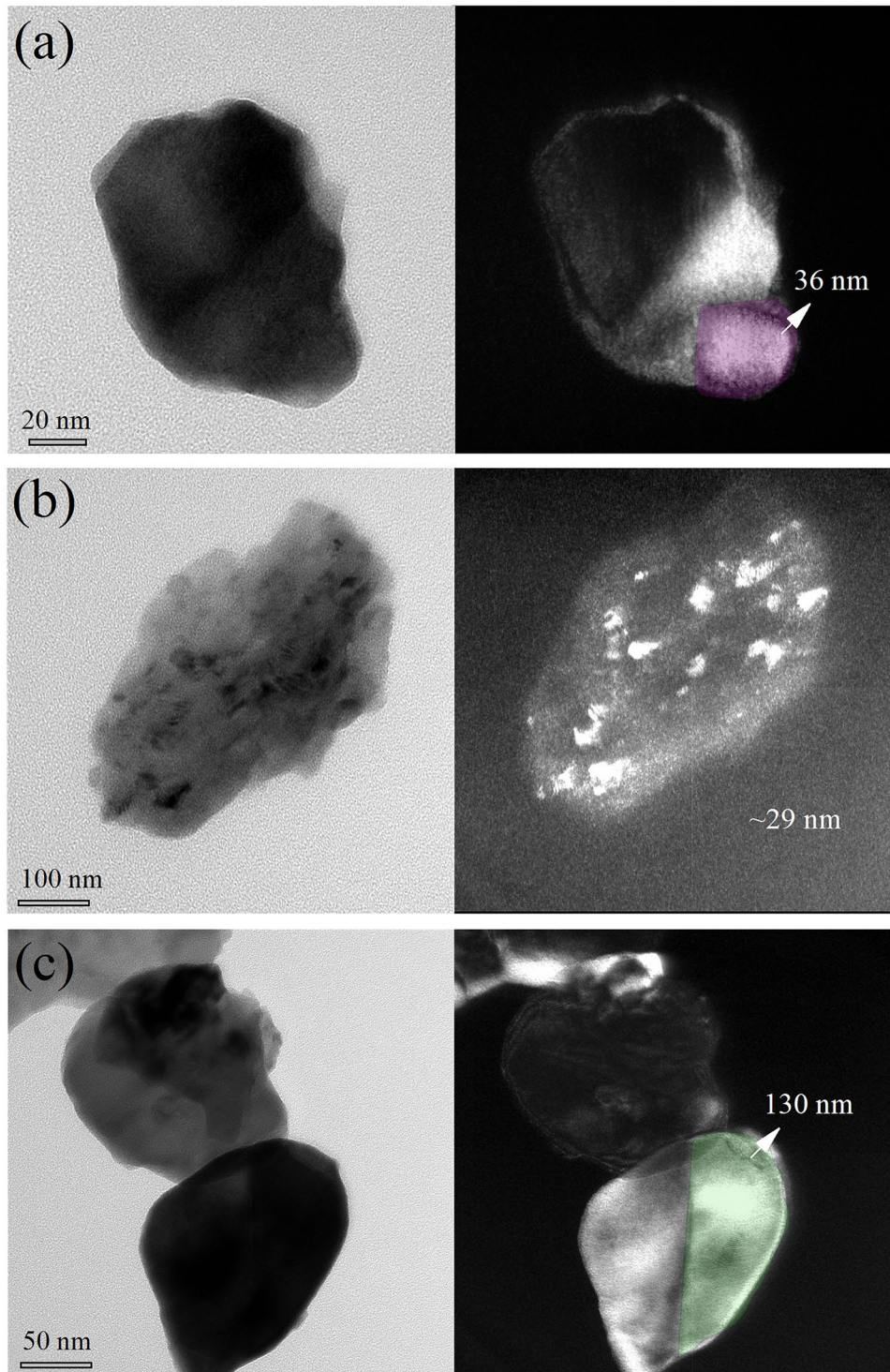


**Fig. 7** Bright and dark-field TEM images for heated (a) pristine  $\text{Bi}_2\text{Te}_{2.7}\text{Se}_{0.3}$ , (b) 0.05wt.%GNS- $\text{Bi}_2\text{Te}_{2.7}\text{Se}_{0.3}$ , and (c) 0.5wt.%GNS- $\text{Bi}_2\text{Te}_{2.7}\text{Se}_{0.3}$

of 0.05wt.% increased the activation energy slightly to 270 kJ/mol, while a higher amount of 0.5wt.% lowered the activation energy greatly to 254 kJ/mol. The obtained data can be explained by understanding the microstructure. Ying et al. [31] calculated the activation energy of grain growth for graphene-doped  $\text{ZrO}_2/\text{Al}_2\text{O}_3$  having different

graphene concentrations (0.2, 0.4, 0.6, and 0.8 vol.%). The authors reported a contentious increase in activation energy as increasing the volume percentage of graphene until an optimum concentration of 0.4 ( $Q(0) = 350.59$  kJ/mol,  $Q(0.2) = 677.12$  kJ/mol,  $Q(0.4) = 753.12$  kJ/mol). However, increasing graphene concentration more than 0.4% caused a

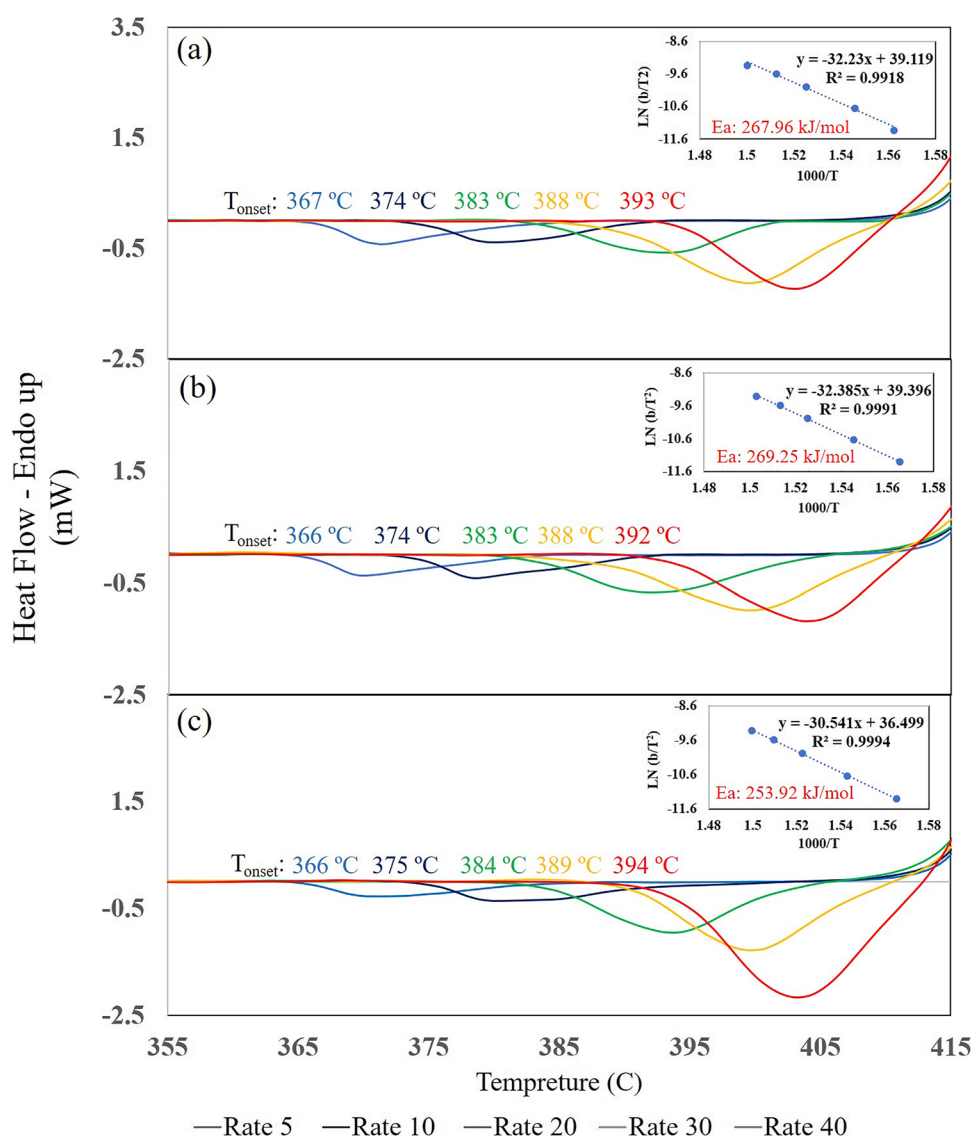


**Fig. 8** Thermal analysis simulation for (a)  $\text{Bi}_2\text{Te}_{2.7}\text{Se}_{0.3}$ , (b) 0.05wt.% Gr- $\text{Bi}_2\text{Te}_{2.7}\text{Se}_{0.3}$ , and (c) 0.5wt.% Gr-  $\text{Bi}_2\text{Te}_{2.7}\text{Se}_{0.3}$  at different heating rates ( $^{\circ}\text{C}/\text{min}$ ); inset: activation energy calculated by the Kissinger method

noticeable drop in the activation energy ( $Q(0.6) = 731.03$  kJ/mol,  $Q(0.8) = 693.58$  kJ/mol). The authors reported that the addition of low amounts of graphene generated a pinning effect, which led to an increase in the potential barrier of mass diffusion [32]. This causes tightness around the grain boundaries that restricted grain growth. This explanation is in good agreement with the relatively high activation energy value in the sample containing 0.05 wt.% GNS (Fig. 8b). Even though 0.05 wt.% of graphene is considered typically low, the corresponding surface area of the two-dimensional graphene nanosheet (unlike 3D particles) is significantly large enough to cover high areas of grain boundaries, thus producing pinning effect. The proposed idea can be visualized more clearly from Fig. 6a, where graphene nanosheets are covering large areas and considerable amount of  $\text{Bi}_2\text{Te}_{2.7}\text{Se}_{0.3}$  particles.

On the other hand, the addition of higher quantities of graphene caused agglomeration of the 2D sheets, as observed in the SEM in Fig. 1d, degrading the pinning effect and allowing for an ease in grain growth. It can be suggested that agglomeration may lead to large pores in composites, which provides more growth spaces for grains, thus lowering the activation energy. Moreover, Zhang et al. [21] proposed that, based on structural analysis, the particle size of the powder (agglomeration) determines the final grain size after the heat treatment. Thus, agglomerated particles tend to encounter grain growth faster than without agglomeration. This could be another reason explaining the relatively low activation energy of grain growth in the sample with high GNS agglomeration (0.5 wt.% Gr-  $\text{Bi}_2\text{Te}_{2.7}\text{Se}_{0.3}$ ).



Another possible factor that might be affecting the activation energy is the lattice strain. The 0.05 wt.% Gr-Bi<sub>2</sub>Te<sub>2.7</sub>Se<sub>0.3</sub> sample had the lowest lattice strain (see Table 1), suggesting lower excess energy. Making this sample, which is free of agglomeration and has less milling-induced defects (as discussed in TEM results), more resistant to grain growth. Since the consolidation of the bismuth telluride milled powders is usually done at temperatures between 300 and 450 °C [9–15], the activation energy of Bi<sub>2</sub>Te<sub>2.7</sub>Se<sub>0.3</sub>, which occurs within this range, is a pivotal factor to be considered. Grain boundaries, dislocations, and defects are considered the main building blocks of the structure as they can tremendously affect the way properties are formed and substantially contribute to the final behavior of the material [33]. A high number of grain boundaries and interior defects strengthen the material considerably but tend to decrease the thermal and electrical conductivity of semiconductors. Thus, taking the obtained grain growth data into consideration when consolidating ball-milled n-type bismuth telluride based on the desired properties is crucial as it represents a turning point to the final design of the material.

## 4 Conclusion

In summary, the activation energy of grain growth for n-type Bi<sub>2</sub>Te<sub>2.7</sub>Se<sub>0.3</sub> alloy and two graphene-based composites was calculated by incorporating DSC data with the Kissinger model. The activation energy of the n-type Bi<sub>2</sub>Te<sub>2.7</sub>Se<sub>0.3</sub> alloy was found to be 268 kJ/mol. Moreover, differences in the concentration of graphene lead to changes in the exfoliation and milling-induced defects of the nanosheets. This led to variations in the activation energy of grain growth for the composite samples. It was found that a lower graphene concentration of 0.05 wt.% increases the potential barrier of mass diffusion due to the pinning effect of the well-exfoliated graphene. However, higher amounts lead to agglomerations that eliminated the pinning effect and allowed for an ease in grain growth. The analyses provided could aid future efforts to engineer the consolidation of ball-milled n-type Bi<sub>2</sub>Te<sub>2.7</sub>Se<sub>0.3</sub> alloys.

**Acknowledgements** The statements made herein are solely the responsibility of the authors. The authors acknowledge the technical support from the Central Laboratory Unit (CLU), the Center of Advanced Materials (CAM), and the Chemistry Department at Qatar University.

**Funding** Open Access funding provided by the Qatar National Library. This work was supported by Grant no. NPRP10–0206–170366 and GSRA8-L-1–0414-21013 from Qatar National Research Fund (a member of the Qatar Foundation).

## Declarations

**Competing interests** The authors declare no competing interests.

**Open Access** This article is licensed under a Creative Commons Attribution 4.0 International License, which permits use, sharing, adaptation, distribution and reproduction in any medium or format, as long as you give appropriate credit to the original author(s) and the source, provide a link to the Creative Commons licence, and indicate if changes were made. The images or other third party material in this article are included in the article's Creative Commons licence, unless indicated otherwise in a credit line to the material. If material is not included in the article's Creative Commons licence and your intended use is not permitted by statutory regulation or exceeds the permitted use, you will need to obtain permission directly from the copyright holder. To view a copy of this licence, visit <http://creativecommons.org/licenses/by/4.0/>.

## References

1. I.T. Witting, F. Ricci, T.C. Chasapis, G. Hautier, G.J. Snyder, The thermoelectric properties of n-type bismuth telluride: bismuth selenide alloys Bi<sub>2</sub>Te<sub>3-x</sub>Se<sub>x</sub>, AAAS Research, **2020**,4361703 (2020).
2. S.I. Ahmed, K.A. Mkhoyan, K.M. Youssef, The activation of deformation mechanisms for improved tensile properties in nanocrystalline aluminum. Mater. Sci. Eng. A. **777**, 139069 (2020).
3. P. Bondavalli, Graphene and Related Nanomaterials: Properties and Applications, 1st edn. (Elsevier, 2018), pp. 1–40.
4. R.A. Andrievski, Review of thermal stability of nanomaterials. J. Mater. Sci. **49**(4), 1449 (2014)
5. H. Mamur, M.R.A. Bhuiyan, F. Korkmaz, M. Nil, A review on bismuth telluride (Bi<sub>2</sub>Te<sub>3</sub>) nanostructure for thermoelectric applications. Renew. Sustain. Energy Rev. **82**, 4159–4169 (2018)
6. Z. Soleimani, S. Zoras, B. Ceranic, S. Shahzad, Y. Cui, A review on recent developments of thermoelectric materials for room-temperature applications. Sustainable Energy Technol. Assess. **37**, 100604 (2020).
7. J.Y. Han, J. Byun, Y. Lee, B.J. Choi, H. Kim, S. Oh. Dilatometric analysis of the sintering behavior OF Bi<sub>2</sub>Te<sub>3</sub> thermoelectric powders. **65**(3):1117–20 (2020)
8. R. Abdelatty, A. Khan, M. Yusuf, A. Alashraf, R.A. Shakoore, Effect of silicon nitride and graphene nanoplatelets on the properties of aluminum metal matrix composites, **14**,1898 (2021).
9. K. Ahmad, C. Wan, M.A. Al-Eshaikh, A.N. Kadachi, Enhanced thermoelectric performance of Bi<sub>2</sub>Te<sub>3</sub> based graphene nanocomposites. Appl. Surf. Sci. **474**, 2-8 (2018)
10. Daewoo Suh, Sanghoon Lee, Hyeona Mun, Sung-Hoon Park, Kyu Hyoung Lee, Sung Wng Kim, Jae-Young Choi, Seunghyun Baik, Enhanced thermoelectric performance of Bi<sub>0.5</sub>Sb<sub>1.5</sub>Te<sub>3</sub>-expanded graphene composites by simultaneous modulation of electronic and thermal carrier transport. **13**,67–76 (2015)
11. K.T. Kim, S.Y. Choi, E.H. Shin, K.S. Moon, H.Y. Koo, G.-G. Lee et al., The influence of CNTs on the thermoelectric properties of a CNT/Bi<sub>2</sub>Te<sub>3</sub> composite. Carbon **52**, 541–549 (2013)
12. Ren F., Wang H., Menchhofer P.A., Kiggans J.O. Thermoelectric and mechanical properties of multi-walled carbon nanotube doped Bi<sub>0.4</sub>Sb<sub>1.6</sub>Te<sub>3</sub> thermoelectric material. 2013;103.
13. Q. Lognoné, F. Gascoin, On the effect of carbon nanotubes on the thermoelectric properties of n-Bi<sub>2</sub>Te<sub>2.4</sub>Se<sub>0.6</sub> made by mechanical alloying. J. Alloys. Compd. **635**, 107–11 (2015)
14. D.-H. Park, M.-Y. Kim, T.-S. Oh, Thermoelectric energy-conversion characteristics of n-type Bi<sub>2</sub>(Te, Se)<sub>3</sub> nanocomposites processed with carbon nanotube dispersion. Curr. Appl. Phys. **11**(4), S41–S45 (2011)

15. Popov M, Buga S, Vysikaylo P, Stepanov P, Skok V, Medvedev V, et al. C60-doping of nanostructured Bi-Sb-Te thermoelectrics 208:2783–9 (2011)
16. S.A. Humphry-Baker, C.A. Schuh, Grain growth and structural relaxation of nanocrystalline Bi<sub>2</sub>Te<sub>3</sub>. *J. Appl. Phys.* **116**(15), 153502 (2014)
17. D. Jang, M. Atzmon, Grain-boundary relaxation and its effect on plasticity in nanocrystalline Fe. *J. Appl. Phys.* **99**(8), 083504 (2006)
18. Metals handbook / prepared under the direction of the ASM International Handbook Committee. 1990. 0–2.
19. T. Degen, M. Sadki, E. Bron, U. König, G. Nénert, The HighScore suite. *Powder. Diffract.* **29**(S2), S13–S8 (2014)
20. X. Wang, J. Zhao, E. Cui, H. Liu, Y. Dong, Z. Sun, Effects of sintering parameters on microstructure, graphene structure stability and mechanical properties of graphene reinforced Al<sub>2</sub>O<sub>3</sub>-based composite ceramic tool material. *Ceram. Int.* **45**(17 Part B), 23384–92 (2019)
21. Q. Zhang, Q. Zhang, S. Chen, W. Liu, K. Lukas, X. Yan et al., Suppression of grain growth by additive in nanostructured p-type bismuth antimony tellurides. *Nano Energy* **1**(1), 183–189 (2012)
22. Neikov OD. Chapter 3 - Mechanical Alloying 2019 Tue Jan 01 00:00:00 AST 2019. 91–124 p.
23. S.I. Ahmad, H. Hamoudi, A. Zekri, K.M. Youssef, Investigating the thermal stability of nanocrystalline aluminum-lithium alloy by combining different mechanisms: reinforcing with graphene and alloying with Sr. *J. Alloy. Compd.* **914**, 165348 (2022)
24. J. Pelleg, in *Mechanical Properties of Materials*, ed. By G.M.L. GLADWELL (Springer, 2013), p. 195.
25. L-S. Lin, AVK. Westwood, R. Drummond-Brydson, Graphene Synthesis via electrochemical exfoliation of graphite nanoplatelets in aqueous sulphuric acid. (White Rose Research Online, 2016), <https://eprints.whiterose.ac.uk/102051/>. Accessed 19 May 2016
26. K.S. Munir, C. Wen, Deterioration of the strong sp<sup>2</sup> carbon network in carbon nanotubes during the mechanical dispersion processing—a review. *Crit. Rev. Solid State Mater. Sci.* **41**(5), 347–366 (2016)
27. B. Marinkovic, R.R.D. Avillez, A. Saavedra, F.C.R. Assunção, A comparison between the Warren-Averbach method and alternate methods for x-ray diffraction microstructure analysis of polycrystalline specimens. *Mater. Res.* **4**(2), 71–6 (2001)
28. S. Vyazovkin, Kissinger Method in kinetics of materials: things to beware and be aware of *Molecules.* **25**:(2813) (2020)
29. L. Hu, T. Zhu, X. Liu, X. Zhao, Point defect engineering of high-performance bismuth-telluride-based thermoelectric materials **24**(5211), 8 (2014)
30. S.A. Humphry-Baker, C.A. Schuh, Anomalous grain refinement trends during mechanical milling of Bi<sub>2</sub>Te<sub>3</sub>. *Acta. Mater.* **75**, 167–179 (2014)
31. Y. Liu, Y. Ai, W. He, W. Chen, J. Zhang, Grain growth kinetics in microwave sintered graphene platelets reinforced ZrO<sub>2</sub>/Al<sub>2</sub>O<sub>3</sub> composites **44**(14):16421–7 (2018)
32. X. Wang, J. Zhao, E.Cui, Z. Sun, H. Yu, Grain growth kinetics and grain refinement mechanism in Al<sub>2</sub>O<sub>3</sub>/WC/TiC/graphene ceramic composite **41**(2):1391–8 (2021).
33. Pavel Lejcek, Grain boundary segregation in metals, (Springer, Dordrecht, 2010), p.1.